文章编号：1001-9014(2019)06-0701-05

DOI:10.11972/j.issn.1001-9014.2019.06.004

Generation of an intensity-balanced optical pulse couple based on silica planar lightwave circuit

REN Mei-Zhen[1,2], LI Xiao[1,2], ZHANG Jia-Shun[1*], WANG Liang-Liang[1], WANG Yue[1], YIN Xiao-Jie[1], WU Yuan-Da[1,2], AN Jun-Ming[1,2*]

(1. State Key Laboratory on Integrated Optoelectronics, Institute of Semiconductors, Chinese Academy of Sciences, Beijing 100083, China;
2. Center of Materials Science and Optoelectronics Engineering, University of Chinese Academy of Sciences, Beijing 100049, China)

Abstract: To make the pulse couple balanced, an asymmetric Mach-Zehnder interferometer (AMZI) with a tunable directional coupler (DC) of a silica-based planar lightwave circuit (PLC) technology was proposed. The simulation results show that the DC tuning effect is better when the refractive index of both coupling arms changes independently. When the distance between the electrode and the waveguide core in the coupling zone is 0, the temperature difference between the coupling arms reaches the maximum. The test results of AMZI show that the insertion loss is 2.05 dB and the delay time is 151.4 ps. The power ratio of the pulse couple is highly close to one. Our device presents a practical solution to improve the performance of future integrated QKD device.

Key words: asymmetric Mach-Zehnder interferometer, thermal field simulation, quantum key distribution

PACS: 42.82.Bq, 42.82.Et, 03.67.Hk

基于二氧化硅平面光波导的强度均衡的光脉冲对的产生

任梅珍[1,2], 李 骁[1,2], 张家顺[1*], 王亮亮[1], 王 玥[1], 尹晓杰[1], 吴远大[1,2], 安俊明[1,2*]

(1. 中国科学院半导体研究所 集成光电子学国家重点实验室,北京 100083;
2. 中国科学院大学 材料科学与光电技术学院,北京 100049)

摘要:提出了一种基于平面光波导工艺的带有可调定向耦合器的非对称MZI结构.模拟结果显示,当定向耦合器的两个耦合臂的折射率独立改变时,定向耦合器的调制效果较好;当调制电极与耦合区的波导间距为0时,两个耦合臂的温度差达到最大.测试得到,AMZI的插入损耗为2.05 dB,延迟时间为151.4 ps,脉冲对的功率比近似为1.该器件有助于提高集成QKD器件的性能.

关 键 词:非对称MZI干涉仪;热场模拟;量子密钥分发

中图分类号:TN256 **文献标识码**:A

Introduction

In recent years, QKD has been developing rapidly which provides an unconditional secure approach to sharing random encryption keys by transmitting single photons[1-3]. BB84 protocol[4-5] is one of the most widely studied protocols up to the present. An AMZI is indispensable in the generation of a time-bin pulse couple to encode or decode the quantum information. Quantum interference has been reported in a free space AMZI configurations[6]. However, bulky optics presents weak consistency. Integrated optical circuits[7] for quantum communication devices show advances of miniaturization, low cost and reconfigurability. So this paper demonstrates an AMZI based on silica PLC technology.

For the AMZI, an optical delay line with delay time

Received date: 2019-03-19, **revised date**: 2009-09-10 **收稿日期**:2019-03-19,**修回日期**:2009-09-10

Foundation items: Supported by National Key R &D Program of China (2018YFA0306403), National Nature Science Foundation of China (61805232, 61435013), and K. C. Wong Education Foundation.

Biography: REN Mei-Zhen (1987-), female, Hebi, China, Ph. D student. Mainly engaged in the research of MZI based on planar lightwave circuit and quantum key distribution. E-mail: renmeizhen@semi.ac.cn

* **Corresponding author**: zhangjiashun@semi.ac.cn, junming@semi.ac.cn

Δt in one of the arms defines the path-length asymmetry[8]. When a short optical pulse with a width much narrower than Δt is launched into an input port of AMZI, a pair of optical pulses with delay time of Δt are exported on its two output ports. In QKD systems, the two output pulses should have equivalent intensity in order to reduce the QBER and improve the performance of the whole system[9]. However, the optical transmission loss is asymmetric for two arms with different length in the AMZI, so one of the couplers in the AMZI should be made slightly asymmetric to compensate for asymmetrical optical transmission loss. One solution is to design asymmetric couplers to match the different losses for the long and short arms[8]. It is necessary to do a mass of experiments to obtain balanced optical pulse couple because the optical loss is hard to predict precisely in advance. Another solution is to use a combination of variable optical attenuator (VOA) and AMZI which will increase the size of the device[3]. Hence tunable couplers are of great importance in the AMZI. They can also be used to increase design and fabrication tolerances of devices[10]. This paper presents an AMZI with tunable directional coupler using the silica-based thermo-optic effect.

1 Theoretical analysis

The schematic diagram of an AMZI is shown in Fig. 1, which can be fabricated using the silica-based PLC technology. The width of the waveguide core is 4 μm. The refractive index for the waveguide core and the cladding are taken as 1.474 49 and 1.444 7 respectively, at an operating wavelength of 1.55 μm. In Fig. 1, the black bold line represents the waveguide core, the green part represents the heating electrode, and the blue part represents the lead electrode. The arm length difference Δl of AMZI can be calculated by the formula

$$\Delta l = c\Delta t/n \quad , \quad (1)$$

where c is the velocity of light in vacuum, Δt is the delay time of AMZI, n is the refractive index of the waveguide core. So the Δl of delay time 150 ps-AMZI is 30.52 mm. When an optical pulse with a width much narrower than Δt is launched into an input port of AMZI, a pulse couple with delay time of Δt is exported through an output port. This is because the two arms of AMZI have different length, so that the separated two pulses at the first DC will not interference at the second DC, but will export with delay time of Δt.

Figure 2 shows a schematic of a DC, The coupling zone is the red part which comprises the up and down arm. The separation between the two arms is 2.0 μm.

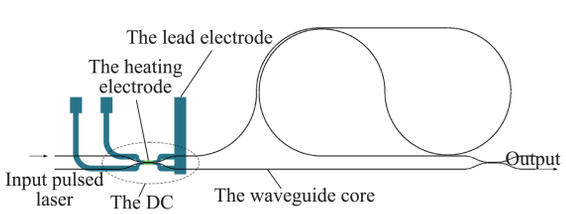

Fig. 1 The schematic diagram of the 150 ps-AMZI
图1 150 ps-AMZI的结构示意图

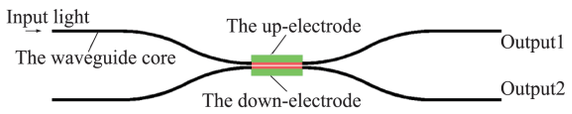

Fig. 2 The schematic diagram of the directional coupler
图2 定向耦合器的结构示意图

The coupling ratio varies with the length of the coupling zone L.

Under the current conditions, the coupling ratio is 3 dB when the length of the coupling zone L is 370 μm. In order to achieve the best tuning effect, we use the Rsoft Photonic Suite to simulate the 3 dB DC under different tuning conditions. The first condition is that the refractive index of both coupling arms changes simultaneously. As shown in Fig. 2, we set the refractive index difference of the red parts are both *delta*+x, then we fix delta as 0.029 79 and scan x in the simulation. The simulation results are shown in Fig. 3. When x changes from 0 to 0.000 5, the difference of the insertion loss between two output channels changes from 0.07 dB to 0.285 dB.

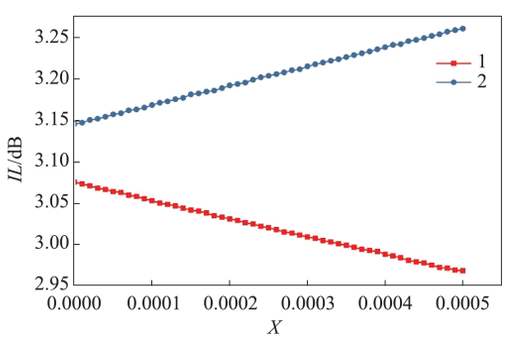

Fig. 3 The insertion loss of two output channels versus x when the refractive index of both coupling arms changes simultaneously
图3 当耦合臂的折射率同时改变时,两个输出通道的插入损耗随x的变化

The second condition is that the refractive index of both coupling arms changes independently. In the simulation, the refractive index difference of the up and down arm of the coupling zone is set as *delta*+x independently, and then we scan x. The simulation results are shown in Fig. 4. No matter which arm is tuned, when x changes from 0 to 0.0005, the difference of the insertion loss between the two output channels changes from 0.07 dB to 0.59 dB. Note that the insertion loss of channel 2 is always greater than that of channel 1.

Comparing the two tuning conditions, the tuning effect of the second condition is better. In order to make the two coupling arms to be tuned independently, it is necessary to maximize the temperature difference between the two arms by thermo-optic effect. Here we simulate the heat field profile of the waveguide under different situations using the finite element analysis.

The structure diagram used in the simulation is shown in Fig. 5. The thickness of the substrate, the down-cladding and the up-cladding is 625 μm, 20 μm, 18 μm respectively. The black parts are the waveguide

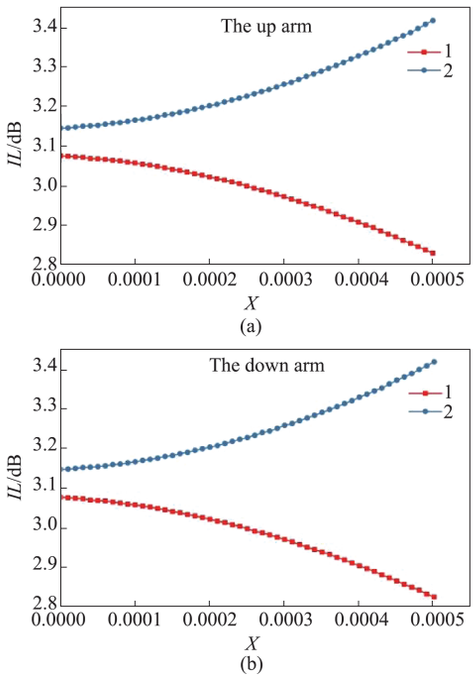

Fig. 4 The insertion loss of two output channels versus x when the refractive index of the two coupling arms change independently (a) when the up arm is tuned, (b) when the down arm is tuned
图4 当耦合臂的折射率分别改变时,两个输出通道的插入损耗随x的变化(a)调节上臂,(b)调节下臂

core in the coupling zone. The height and width of the waveguide core are both 4 μm. The separation between the two arms in the coupling zone is 2 μm. The length of the two arms is 370 μm. The green part is the tuning electrode. The width and thickness of the electrode are 15 μm and 0.3 μm respectively. The electrode material in the simulation is tungsten. The thermal conductivity of tungsten is 174 W/m · K. The distance between the electrode and the waveguide core is d. In the simulation the heat flow is supplied to the electrode and the temperature of the substrate is set at the room temperature 22℃. We monitor the temperature of the two coupling arms when changing the position of the electrode (under different values of d) and supplying different heat flow to the electrode. The simulation results are shown in Fig. 6. When the electrode is at a fixed position, the temperature difference between the two arms increases linearly with the heat flow. Generally, the thermo-optic coefficient of SiO_2 is 1.19×10^{-5} K^{-1}, so the refractive index difference between the two arms increases linearly with the heat flow. The temperature difference between the two arms reaches the maximum when d=0. If we set the temperature difference between the two arms and heat flow as ΔT and H, respectively, the fitting curve shows that ΔT=0.077 H, provided d=0. The dependency of ΔT with respect to d is shown in Fig. 7, under the heat flow of 100 mW.

As shown in Fig. 2, the length of the electrode is the same as that of the coupling zone. The distance between the electrode and the waveguide core is 0. The up-electrode and down-electrode are separately arranged.

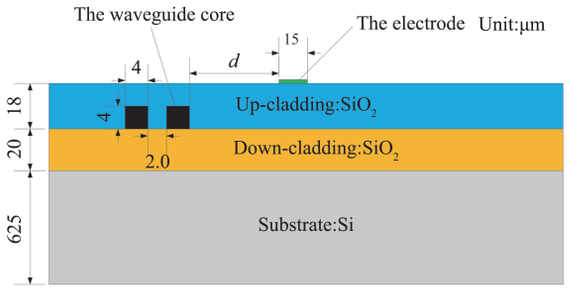

Fig. 5 The structure diagram of the coupling zone of the directional coupler in the thermal analysis
图5 在热分析中定向耦合器的耦合区的横截面示意图

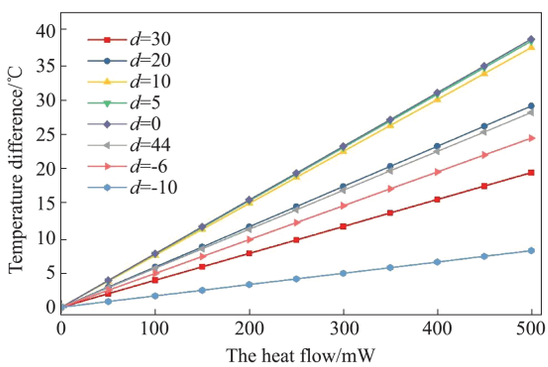

Fig. 6 The temperature difference between the two arms versus the heat flow when d is different values (unit: μm)
图6 当d是不同值时,两个耦合臂之间的温度差随着功耗的变化

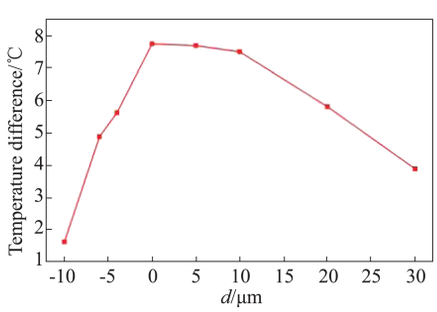

Fig. 7 The temperature difference between the two arms versus d when the heat flow is 100 mW
图7 当功耗是100 mW时,两个耦合臂之间的温度差随着d的变化

2 Experiment

We use conventional silica-based PLC technology to fabricate our device. This technology consists of thermal oxidation, PECVD deposition, photolithography and ICP etching, Boro-Phospho-Silicate-Glass (BPSG) overcladding deposition and annealing, and so on. First, 1050 ℃ thermal oxidation is used to form 16 μm thick down cladding, Plasma Enhanced Chemical Vapor Deposition (PECVD) is used to form 4 μm-thick GeO_2-SiO_2 core, contact exposure photolithography and ICP etching are used to fulfill pattern transfer. PECVD is used to form 20 μm-thick BPSG upper cladding, at last thin film heaters are deposited by means of magnetron sputtering.

In order to investigate the effect of the tuning electrode, we firstly fabricated a directional coupler with the coupling zone length of 370 μm. To tune the coupling ratio, one of the electrodes was connected to a direct-current power supply.

A laser beam with a wavelength 1.55 μm and a linewidth of less than 5 MHz is input to the directional coupler, while the two output channels are simultaneously monitored by the dual-channel power meter. We measure the output power of two channels while various voltages are loaded on the electrode. Figure 8 shows the curves of insertion loss versus the tuning current.

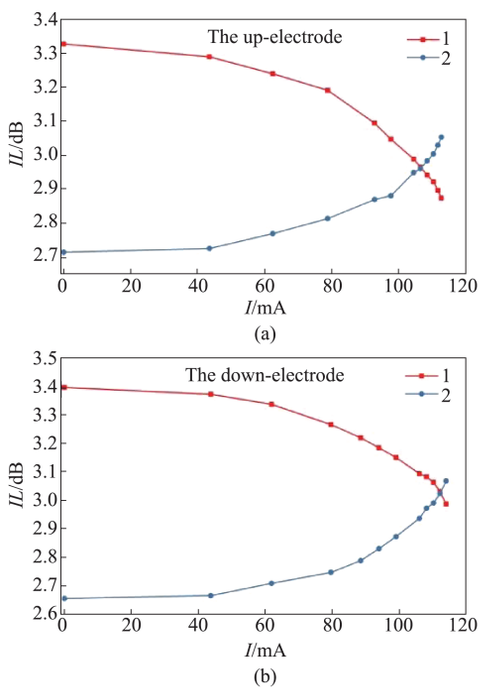

Fig. 8 Insertion loss versus the tuning current (a) the up-electrode is tuned, and (b) the down-electrode is tuned
图8 插入损耗随着加载电流的变化(a)调节上电极,(b)调节下电极

For channel 1, the insertion loss decreases with the tuning current, when either the up-electrode or the down-electrode is tuned. However, for channel 2 the insertion loss always increases with the tuning current, no matter which electrode is tuned. Within the tuning range of 120 mA, the insertion loss of channel 1 changes from 3.32 dB to 2.87 dB, achieving the tuning range of 0.45 dB. Similarly the insertion loss of channel 2 changes from 2.65 dB to 3.06 dB, achieving the tuning range of 0.41 dB.

Although the tuning range of 0.4 dB is small, it is sufficient in the application of AMZI. Generally, the arm length difference of AMZI is less than 100 mm. So the transmission loss difference of the two arms is less than 0.35 dB. For the AMZI in this paper, the arm length difference of 150 ps delay is about 30 mm. The transmission loss difference of the two arms is less than 0.11 dB under the current fabrication process.

The fabricated AMZI is shown in Fig. 9. The size of this AMZI is 16.8 mm×4.6 mm. And its insertion loss is 2.05 dB which is defined as the ratios of the input power coupled to the chip and the total output power of the two output ports. To test the performance, the AMZI is connected as Fig. 10. The input and output ports are connected as Fig. 1. The pulsed laser outputs light with pulse width 50 ps and frequency 500 MHz. The high-speed oscilloscope is operated at 33 GHz. The tuning electrode of the directional coupler is connected to a direct-current power supply. When a pulsed light is input to the AMZI, a pulse couple is exported at the output port due to the asymmetry of the two arms.

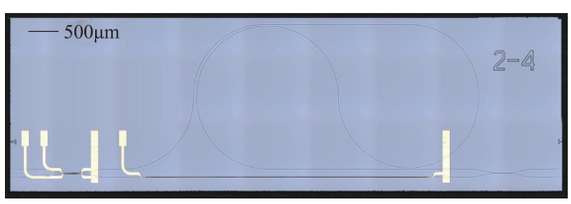

Fig. 9 The micrograph of the fabricated AMZI
图9 制备的AMZI的显微镜照片

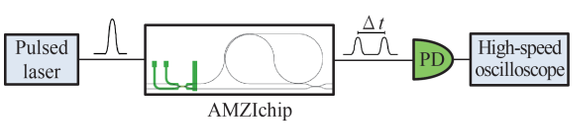

Fig. 10 The test block diagram of the pulse couple
图10 脉冲对的测试框图

When no voltage is applied on the electrode, the pulse couple is shown in Fig. 11. The oscilloscope output of the first pulse is V_1(99.24 mV)and the second pulse is V_2(97.32mV). The delay time between the first and the second pulse is measured as 151.4 ps. This value is approximately equal to the theoretical value, which is within the allowed error range. In order to compare the two pulses, we draw the curves of V_1/V_2 versus the tuning current. It is obvious that the tuning effect is best when V_1/V_2 =1. The first pulse is transmitted from the shorter arm in the AMZI and the second pulse is transmitted from the longer arm.

When different voltages are applied on the elec-

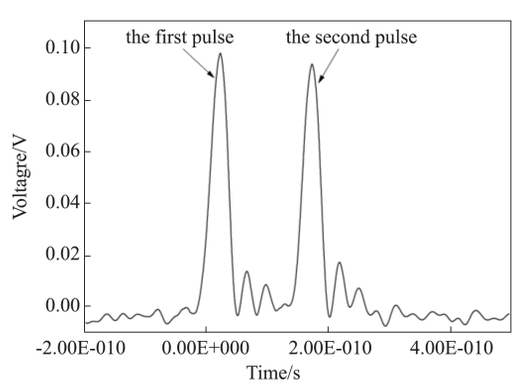

Fig. 11 The output pulse couple when no voltage is applied
图11 当不加载电压时,输出的脉冲对

trodes of the directional coupler, the curves of V_1/V_2 versus the tuning current are shown in Fig. 12. When the current on the up electrode is 60 mA, the two pulses achieve the most balanced state. The ratio of V_1/V_2 is 1.009. When the current on the down electrode is 70 mA, the two pulses achieve the most balanced state. The ratio of V_1/V_2 is 1.004. The balanced state is shown in Fig. 13. V_1 and V_2 are 102.67 mV, 102.22 mV, respectively. The results show that a tunable directional coupler can tune the splitting ratio between the longer and shorter arms in the AMZI effectively.

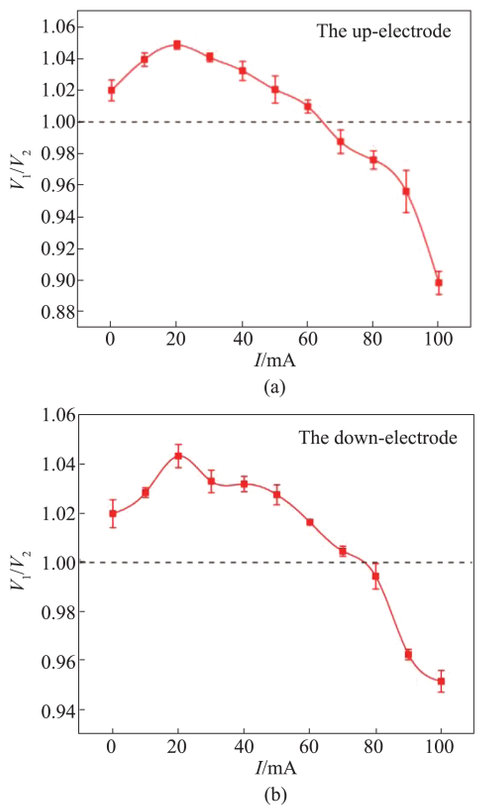

Fig. 12 V_1/V_2 versus the tuning current (a) the up-electrode is tuned, (b) the down-electrode is tuned
图12 V_1/V_2 随着加载电流的变化(a)调节上电极,(b)调节下电极

3 Conclusion

In summary, we have presented an AMZI which can output intensity-balanced pulse couple. The insertion loss is 2.05 dB. The delay time between the first and the second pulse is 151.4 ps. The power ratio of the pulse couple is highly close to one. Our device has shown a good tuning ability, thus presenting great potential to improve the visibility of quantum interference and reduce the QBER.

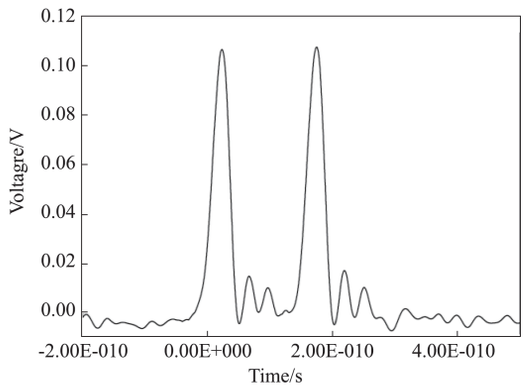

Fig. 13 The output pulse couple at the balanced state
图13 输出的平衡脉冲对

References

[1] Kennard J E, Sibson P, Stanisic S, *et al*. Integrated Silicon Photonics for High-Speed Quantum Key Distribution[C]. *Conference on Lasers and Electro-Optics*, 2017: JTh3E.4.
[2] Ma C, Sacher W D, Tang Z, *et al*. Silicon photonic transmitter for polarization-encoded quantum key distribution [J]. *Optica*, 2016, **3**(11): 1274-1278.
[3] Sibson P, Erven C, Godfrey M, *et al*. Chip-based quantum key distribution [J]. *Nature Communications*, 2017, **8**: 13984.
[4] Bennett C H, Brassard G. Quantum cryptography: Public key distribution and coin tossing [J]. *Theoretical Computer Science*, 2014, **560**: 7-11.
[5] Nambu Y, Yoshino K i, Tomita A. One-way quantum key distribution system based on planar lightwave circuits [J]. *Japanese Journal of Applied Physics*, 2006, **45**(6A): 5344-5348.
[6] Trenti A, Borghi M, Mancinelli M, *et al*. Quantum interference in an asymmetric Mach-Zehnder interferometer [J]. *Journal of Optics*, 2016, **18**(8): 085201.
[7] Bonneau D, Silverstone J W, Santagati R, *et al*. Silicon quantum photonics. *In* 2015 *European Conference on Lasers and Electro-Optics - European Quantum Electronics Conference*, 2015: JSV_1_1.
[8] Nambu Y, Yoshino K i, Tomita A. Quantum encoder and decoder for practical quantum key distribution using a planar lightwave circuit [J]. *Journal of Modern Optics*, 2008, **55**(12): 1953-1970.
[9] Gobby C, Yuan Z L, Shields A J. Quantum key distribution over 122 km of standard telecom fiber [J]. *Applied Physics Letters*, 2004, **84**(19): 3762-3764.
[10] Orlandi P, Morichetti F, Strain M J, *et al*. Tunable silicon photonics directional coupler driven by a transverse temperature gradient [J]. *Optics Letters*, 2013, **38**(6): 863-865.